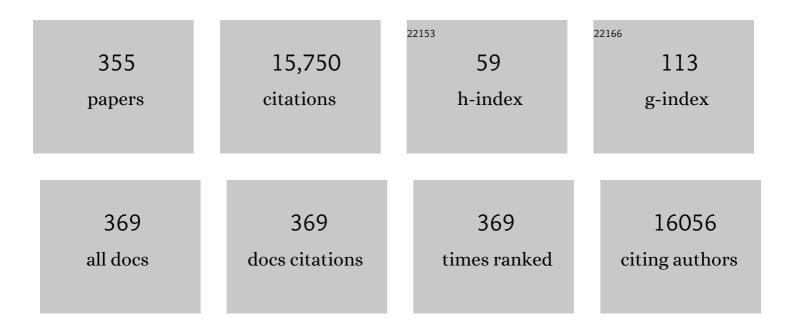
List of Publications by Year in descending order

Source: https://exaly.com/author-pdf/9204339/publications.pdf Version: 2024-02-01



IAN SUREDS

#	Article	IF	CITATIONS
1	Denoising of diffusion MRI using random matrix theory. NeuroImage, 2016, 142, 394-406.	4.2	1,208
2	Multi-tissue constrained spherical deconvolution for improved analysis of multi-shell diffusion MRI data. NeuroImage, 2014, 103, 411-426.	4.2	1,063
3	Investigating the prevalence of complex fiber configurations in white matter tissue with diffusion magnetic resonance imaging. Human Brain Mapping, 2013, 34, 2747-2766.	3.6	887
4	The ASTRA Toolbox: A platform for advanced algorithm development in electron tomography. Ultramicroscopy, 2015, 157, 35-47.	1.9	652
5	Fast and flexible X-ray tomography using the ASTRA toolbox. Optics Express, 2016, 24, 25129.	3.4	638
6	Weighted linear least squares estimation of diffusion MRI parameters: Strengths, limitations, and pitfalls. NeuroImage, 2013, 81, 335-346.	4.2	407
7	Probabilistic fiber tracking using the residual bootstrap with constrained spherical deconvolution. Human Brain Mapping, 2011, 32, 461-479.	3.6	335
8	Maximum-likelihood estimation of Rician distribution parameters. IEEE Transactions on Medical Imaging, 1998, 17, 357-361.	8.9	325
9	Gliomas: Diffusion Kurtosis MR Imaging in Grading. Radiology, 2012, 263, 492-501.	7.3	311
10	Performance improvements for iterative electron tomography reconstruction using graphics processing units (GPUs). Journal of Structural Biology, 2011, 176, 250-253.	2.8	292
11	3D imaging of nanomaterials by discrete tomography. Ultramicroscopy, 2009, 109, 730-740.	1.9	255
12	DART: A Practical Reconstruction Algorithm for Discrete Tomography. IEEE Transactions on Image Processing, 2011, 20, 2542-2553.	9.8	253
13	Estimation of the Noise in Magnitude MR Images. Magnetic Resonance Imaging, 1998, 16, 87-90.	1.8	245
14	Maximum likelihood estimation of signal amplitude and noise variance from MR data. Magnetic Resonance in Medicine, 2004, 51, 586-594.	3.0	236
15	L1 knockout mice show dilated ventricles, vermis hypoplasia and impaired exploration patterns. Human Molecular Genetics, 1998, 7, 999-1009.	2.9	228
16	Reduction of ring artefacts in high resolution micro-CT reconstructions. Physics in Medicine and Biology, 2004, 49, N247-N253.	3.0	210
17	More accurate estimation of diffusion tensor parameters using diffusion kurtosis imaging. Magnetic Resonance in Medicine, 2011, 65, 138-145.	3.0	202
18	Optimal Experimental Design for Diffusion Kurtosis Imaging. IEEE Transactions on Medical Imaging, 2010, 29, 819-829.	8.9	180

#	Article	IF	CITATIONS
19	Extraction of Airways From CT (EXACT'09). IEEE Transactions on Medical Imaging, 2012, 31, 2093-2107.	8.9	173
20	StatSTEM: An efficient approach for accurate and precise model-based quantification of atomic resolution electron microscopy images. Ultramicroscopy, 2016, 171, 104-116.	1.9	170
21	Automatic estimation of the noise variance from the histogram of a magnetic resonance image. Physics in Medicine and Biology, 2007, 52, 1335-1348.	3.0	139
22	Watershed-based segmentation of 3D MR data for volume quantization. Magnetic Resonance Imaging, 1997, 15, 679-688.	1.8	133
23	Quantitative diffusion tensor imaging in amyotrophic lateral sclerosis: Revisited. Human Brain Mapping, 2009, 30, 3657-3675.	3.6	122
24	Diffusion kurtosis imaging probes cortical alterations and white matter pathology following cuprizone induced demyelination and spontaneous remyelination. NeuroImage, 2016, 125, 363-377.	4.2	122
25	Diffusion kurtosis imaging allows the early detection and longitudinal follow-up of amyloid-β-induced pathology. Alzheimer's Research and Therapy, 2018, 10, 1.	6.2	120
26	Limbic and Callosal White Matter Changes in Euthymic Bipolar I Disorder: An Advanced Diffusion Magnetic Resonance Imaging Tractography Study. Biological Psychiatry, 2013, 73, 194-201.	1.3	116
27	The effect of spaceflight and microgravity on the human brain. Journal of Neurology, 2017, 264, 18-22.	3.6	113
28	Measuring Lattice Strain in Three Dimensions through Electron Microscopy. Nano Letters, 2015, 15, 6996-7001.	9.1	110
29	Machine learning study of several classifiers trained with texture analysis features to differentiate benign from malignant softâ€ŧissue tumors in T1â€MRI images. Journal of Magnetic Resonance Imaging, 2010, 31, 680-689.	3.4	106
30	Magnetic Resonance Imaging and Spectroscopy Reveal Differential Hippocampal Changes in Anhedonic and Resilient Subtypes of the Chronic Mild Stress Rat Model. Biological Psychiatry, 2011, 70, 449-457.	1.3	106
31	Nonrigid Coregistration of Diffusion Tensor Images Using a Viscous Fluid Model and Mutual Information. IEEE Transactions on Medical Imaging, 2007, 26, 1598-1612.	8.9	105
32	Cortical reorganization in an astronaut's brain after long-duration spaceflight. Brain Structure and Function, 2016, 221, 2873-2876.	2.3	103
33	Iterative correction of beam hardening artifacts in CT. Medical Physics, 2011, 38, S36-S49.	3.0	100
34	Integration of TomoPy and the ASTRA toolbox for advanced processing and reconstruction of tomographic synchrotron data. Journal of Synchrotron Radiation, 2016, 23, 842-849.	2.4	100
35	Parameter estimation from magnitude MR images. International Journal of Imaging Systems and Technology, 1999, 10, 109-114.	4.1	97
36	Brain ventricular volume changes induced by long-duration spaceflight. Proceedings of the National Academy of Sciences of the United States of America, 2019, 116, 10531-10536.	7.1	94

#	Article	IF	CITATIONS
37	Comparing isotropic and anisotropic smoothing for voxelâ€based DTI analyses: A simulation study. Human Brain Mapping, 2010, 31, 98-114.	3.6	89
38	Comprehensive framework for accurate diffusion MRI parameter estimation. Magnetic Resonance in Medicine, 2013, 70, 972-984.	3.0	89
39	Quantitative Three-Dimensional Reconstruction of Catalyst Particles for Bamboo-like Carbon Nanotubes. Nano Letters, 2007, 7, 3669-3674.	9.1	88
40	Brain Tissue–Volume Changes in Cosmonauts. New England Journal of Medicine, 2018, 379, 1678-1680.	27.0	88
41	Unsupervised Retinal Vessel Segmentation Using Combined Filters. PLoS ONE, 2016, 11, e0149943.	2.5	81
42	Noise measurement from magnitude MRI using local estimates of variance and skewness. Physics in Medicine and Biology, 2010, 55, N441-N449.	3.0	80
43	Mathematical framework for simulating diffusion tensor MR neural fiber bundles. Magnetic Resonance in Medicine, 2005, 53, 944-953.	3.0	77
44	Constrained maximum likelihood estimation of the diffusion kurtosis tensor using a Rician noise model. Magnetic Resonance in Medicine, 2011, 66, 678-686.	3.0	77
45	On the construction of an inter-subject diffusion tensor magnetic resonance atlas of the healthy human brain. NeuroImage, 2008, 43, 69-80.	4.2	76
46	Dynamic intensity normalization using eigen flat fields in X-ray imaging. Optics Express, 2015, 23, 27975.	3.4	74
47	Quantification and improvement of the signal-to-noise ratio in a magnetic resonance image acquisition procedure. Magnetic Resonance Imaging, 1996, 14, 1157-1163.	1.8	73
48	Restoration of MR-induced artifacts in simultaneously recorded MR/EEG data. Magnetic Resonance Imaging, 1999, 17, 1383-1391.	1.8	71
49	Reduction of ECG and gradient related artifacts in simultaneously recorded human EEG/MRI data. Magnetic Resonance Imaging, 2000, 18, 881-886.	1.8	70
50	An energy-based beam hardening model in tomography. Physics in Medicine and Biology, 2002, 47, 4181-4190.	3.0	70
51	A trackingâ€based diffusion tensor imaging segmentation method for the detection of diffusionâ€related changes of the cervical spinal cord with aging. Journal of Magnetic Resonance Imaging, 2008, 27, 978-991.	3.4	70
52	Correlation of cognitive dysfunction and diffusion tensor MRI measures in patients with mild and moderate multiple sclerosis. Journal of Magnetic Resonance Imaging, 2010, 31, 1492-1498.	3.4	70
53	Harmonization of Brain Diffusion MRI: Concepts and Methods. Frontiers in Neuroscience, 2020, 14, 396.	2.8	70
54	Multiscale white matter fiber tract coregistration: A new feature-based approach to align diffusion tensor data. Magnetic Resonance in Medicine, 2006, 55, 1414-1423.	3.0	69

#	Article	IF	CITATIONS
55	Regional gray matter volume differences and sex-hormone correlations as a function of menstrual cycle phase and hormonal contraceptives use. Brain Research, 2013, 1530, 22-31.	2.2	69
56	Spatiotemporal properties of the BOLD response in the songbirds' auditory circuit during a variety of listening tasks. Neurolmage, 2005, 25, 1242-1255.	4.2	65
57	Diffusion tensor imaging in a rat model of Parkinson's disease after lesioning of the nigrostriatal tract. NMR in Biomedicine, 2009, 22, 697-706.	2.8	65
58	Alterations of Functional Brain Connectivity After Long-Duration Spaceflight as Revealed by fMRI. Frontiers in Physiology, 2019, 10, 761.	2.8	63
59	Neuroanatomy of the fragile X knockout mouse brain studied using in vivo high resolution magnetic resonance imaging. European Journal of Human Genetics, 1999, 7, 526-532.	2.8	61
60	Maximum likelihood estimation-based denoising of magnetic resonance images using restricted local neighborhoods. Physics in Medicine and Biology, 2011, 56, 5221-5234.	3.0	60
61	Data distributions in magnetic resonance images: A review. Physica Medica, 2014, 30, 725-741.	0.7	60
62	Microstructural changes observed with DKI in a transgenic Huntington rat model: Evidence for abnormal neurodevelopment. NeuroImage, 2012, 59, 957-967.	4.2	59
63	Nonlocal maximum likelihood estimation method for denoising multiple-coil magnetic resonance images. Magnetic Resonance Imaging, 2012, 30, 1512-1518.	1.8	59
64	Model-based two-object resolution from observations having counting statistics. Ultramicroscopy, 1999, 77, 37-48.	1.9	57
65	A diffusion tensor imaging group study of the spinal cord in multiple sclerosis patients with and without T ₂ spinal cord lesions. Journal of Magnetic Resonance Imaging, 2009, 30, 25-34.	3.4	57
66	The effect of template selection on diffusion tensor voxel-based analysis results. NeuroImage, 2011, 55, 566-573.	4.2	57
67	Reproducibility and intercorrelation of graph theoretical measures in structural brain connectivity networks. Medical Image Analysis, 2019, 52, 56-67.	11.6	57
68	Adaptive anisotropic noise filtering for magnitude MR data. Magnetic Resonance Imaging, 1999, 17, 1533-1539.	1.8	56
69	Optimal Threshold Selection for Tomogram Segmentation by Projection Distance Minimization. IEEE Transactions on Medical Imaging, 2009, 28, 676-686.	8.9	56
70	Macro- and microstructural changes in cosmonauts' brains after long-duration spaceflight. Science Advances, 2020, 6, .	10.3	56
71	Altered functional brain connectivity in patients with visually induced dizziness. NeuroImage: Clinical, 2017, 14, 538-545.	2.7	55
72	TomoBank: a tomographic data repository for computational x-ray science. Measurement Science and Technology, 2018, 29, 034004.	2.6	55

#	Article	IF	CITATIONS
73	Does the use of hormonal contraceptives cause microstructural changes in cerebral white matter? Preliminary results of a DTI and tractography study. European Radiology, 2013, 23, 57-64.	4.5	54
74	On the construction of a ground truth framework for evaluating voxel-based diffusion tensor MRI analysis methods. NeuroImage, 2009, 46, 692-707.	4.2	52
75	Isotropic non-white matter partial volume effects in constrained spherical deconvolution. Frontiers in Neuroinformatics, 2014, 8, 28.	2.5	51
76	Adaptive thresholding of tomograms by projection distance minimization. Pattern Recognition, 2009, 42, 2297-2305.	8.1	50
77	Superâ€resolution for multislice diffusion tensor imaging. Magnetic Resonance in Medicine, 2013, 69, 103-113.	3.0	50
78	Diffusion Kurtosis Imaging: A Possible MRI Biomarker for AD Diagnosis?. Journal of Alzheimer's Disease, 2015, 48, 937-948.	2.6	50
79	Estimation of unknown structure parameters from high-resolution (S)TEM images: What are the limits?. Ultramicroscopy, 2013, 134, 34-43.	1.9	49
80	Iterative reweighted linear least squares for accurate, fast, and robust estimation of diffusion magnetic resonance parameters. Magnetic Resonance in Medicine, 2015, 73, 2174-2184.	3.0	48
81	Bias Field Correction for MRI Images. Advances in Soft Computing, 2005, , 543-551.	0.4	47
82	Evaluation of an anthropometric shape model of the human scalp. Applied Ergonomics, 2015, 48, 70-85.	3.1	47
83	Diffusion kurtosis imaging to detect amyloidosis in an APP/PS1 mouse model for Alzheimer's disease. Magnetic Resonance in Medicine, 2013, 69, 1115-1121.	3.0	46
84	A segmentation and classification algorithm for online detection of internal disorders in citrus using X-ray radiographs. Postharvest Biology and Technology, 2016, 112, 205-214.	6.0	44
85	Automatic Parameter Estimation for the Discrete Algebraic Reconstruction Technique (DART). IEEE Transactions on Image Processing, 2012, 21, 4608-4621.	9.8	43
86	Accurate segmentation of dense nanoparticles by partially discrete electron tomography. Ultramicroscopy, 2012, 114, 96-105.	1.9	41
87	A new non-local maximum likelihood estimation method for Rician noise reduction in magnetic resonance images using the Kolmogorov–Smirnov test. Signal Processing, 2014, 103, 16-23.	3.7	41
88	Ergonomic design of an EEG headset using 3D anthropometry. Applied Ergonomics, 2017, 58, 128-136.	3.1	41
89	Superâ€resolution reconstruction of diffusion parameters from diffusionâ€weighted images with different slice orientations. Magnetic Resonance in Medicine, 2016, 75, 181-195.	3.0	40
90	An Iterative CT Reconstruction Algorithm for Fast Fluid Flow Imaging. IEEE Transactions on Image Processing, 2015, 24, 4446-4458.	9.8	39

#	Article	IF	CITATIONS
91	Affine Coregistration of Diffusion Tensor Magnetic Resonance Images Using Mutual Information. Lecture Notes in Computer Science, 2005, , 523-530.	1.3	39
92	Dart: A Fast Heuristic Algebraic Reconstruction Algorithm for Discrete Tomography. , 2007, , .		38
93	Quantitative 3D analysis of huge nanoparticle assemblies. Nanoscale, 2016, 8, 292-299.	5.6	38
94	Assessment of Anterior Cruciate Ligament Graft Maturity With Conventional Magnetic Resonance Imaging: A Systematic Literature Review. Orthopaedic Journal of Sports Medicine, 2019, 7, 232596711984901.	1.7	38
95	Nondestructive internal quality inspection of pear fruit by X-ray CT using machine learning. Food Control, 2020, 113, 107170.	5.5	38
96	General and Efficient Super-Resolution Method for Multi-slice MRI. Lecture Notes in Computer Science, 2010, 13, 615-622.	1.3	37
97	The anatomy of the clavicle. Clinical Anatomy, 2014, 27, 712-723.	2.7	36
98	Informed constrained spherical deconvolution (iCSD). Medical Image Analysis, 2015, 24, 269-281.	11.6	36
99	Iterative bilateral filter for Rician noise reduction in MR images. Signal, Image and Video Processing, 2015, 9, 1543-1548.	2.7	35
100	Identification and characterization of Huntington related pathology: An in vivo DKI imaging study. NeuroImage, 2012, 63, 653-662.	4.2	34
101	Product sizing with 3D anthropometry and <mml:math xmlns:mml="http://www.w3.org/1998/Math/MathML" altimg="si4.gif" display="inline" id="mml4" overflow="scroll"> <mml:mi>k</mml:mi>-medoids clustering. CAD Computer Aided Design, 2017. 91. 60-74.</mml:math 	2.7	34
102	Functional Magnetic Resonance Imaging in Zebra Finch Discerns the Neural Substrate Involved in Segregation of Conspecific Song From Background Noise. Journal of Neurophysiology, 2008, 99, 931-938.	1.8	33
103	Population-averaged diffusion tensor imaging atlas of the Sprague Dawley rat brain. NeuroImage, 2011, 58, 975-983.	4.2	33
104	Subcortical volumetric changes across the adult lifespan: Subregional thalamic atrophy accounts for age-related sensorimotor performance declines. Cortex, 2015, 65, 128-138.	2.4	33
105	Threeâ€dimensional quantitative analysis of healthy foot shape: a proof of concept study. Journal of Foot and Ankle Research, 2018, 11, 8.	1.9	33
106	Combination of shape and X-ray inspection for apple internal quality control: in silico analysis of the methodology based on X-ray computed tomography. Postharvest Biology and Technology, 2019, 148, 218-227.	6.0	32
107	Super-Resolution for Computed Tomography Based on Discrete Tomography. IEEE Transactions on Image Processing, 2014, 23, 1181-1193.	9.8	31
108	DART: a robust algorithm for fast reconstruction of three-dimensional grain maps. Journal of Applied Crystallography, 2010, 43, 1464-1473.	4.5	30

#	Article	IF	CITATIONS
109	A complementary diffusion tensor imaging (DTI)-histological study in a model of Huntington's disease. Neurobiology of Aging, 2012, 33, 945-959.	3.1	29
110	Automated correction of improperly rotated diffusion gradient orientations in diffusion weighted MRI. Medical Image Analysis, 2014, 18, 953-962.	11.6	29
111	In-line NDT with X-Ray CT combining sample rotation and translation. NDT and E International, 2016, 84, 89-98.	3.7	29
112	Dissecting cognitive stages with time-resolved fMRI data: a comparison of fuzzy clustering and independent component analysis. Magnetic Resonance Imaging, 2007, 25, 860-868.	1.8	28
113	How to optimize the design of a quantitative HREM experiment so as to attain the highest precision. Journal of Microscopy, 1999, 194, 95.	1.8	26
114	Multisensor X-ray inspection of internal defects in horticultural products. Postharvest Biology and Technology, 2017, 128, 33-43.	6.0	26
115	FleXCT: a flexible X-ray CT scanner with 10 degrees of freedom. Optics Express, 2021, 29, 3438.	3.4	26
116	The effect of prolonged spaceflight on cerebrospinal fluid and perivascular spaces of astronauts and cosmonauts. Proceedings of the National Academy of Sciences of the United States of America, 2022, 119, e2120439119.	7.1	26
117	Special designed RF-antenna with integrated non-invasive carbon electrodes for simultaneous magnetic resonance imaging and electroencephalography acquisition at 7T. Magnetic Resonance Imaging, 2000, 18, 887-891.	1.8	25
118	Optimal experimental design for the detection of light atoms from high-resolution scanning transmission electron microscopy images. Applied Physics Letters, 2014, 105, .	3.3	24
119	X-ray phase contrast simulation for grating-based interferometry using GATE. Optics Express, 2020, 28, 33390.	3.4	24
120	A distributed ASTRA toolbox. Advanced Structural and Chemical Imaging, 2016, 2, 19.	4.0	23
121	Easy implementation of advanced tomography algorithms using the ASTRA toolbox with Spot operators. Numerical Algorithms, 2016, 71, 673-697.	1.9	23
122	Diffusion tensor imaging of the anterior cruciate ligament graft. Journal of Magnetic Resonance Imaging, 2017, 46, 1423-1432.	3.4	23
123	Non-destructive internal disorder detection of Conference pears by semantic segmentation of X-ray CT scans using deep learning. Expert Systems With Applications, 2021, 176, 114925.	7.6	23
124	Generic iterative subset algorithms for discrete tomography. Discrete Applied Mathematics, 2009, 157, 438-451.	0.9	22
125	Automatic Construction of Correspondences for Tubular Surfaces. IEEE Transactions on Pattern Analysis and Machine Intelligence, 2010, 32, 636-651.	13.9	22
126	Optimal Threshold Selection for Segmentation of Dense Homogeneous Objects in Tomographic Reconstructions. IEEE Transactions on Medical Imaging, 2011, 30, 980-989.	8.9	22

#	Article	IF	CITATIONS
127	A semi-automatic algorithm for grey level estimation in tomography. Pattern Recognition Letters, 2011, 32, 1395-1405.	4.2	22
128	Dynamic angle selection in binary tomography. Computer Vision and Image Understanding, 2013, 117, 306-318.	4.7	22
129	Correspondence Preserving Elastic Surface Registration with Shape Model Prior. , 2014, , .		21
130	Fast Fourier-Based Phase Unwrapping on the Graphics Processing Unit in Real-Time Imaging Applications. Journal of Imaging, 2015, 1, 31-44.	3.0	20
131	Inline discrete tomography system: Application to agricultural product inspection. Computers and Electronics in Agriculture, 2017, 138, 117-126.	7.7	20
132	Diffusion kurtosis imaging with free water elimination: A bayesian estimation approach. Magnetic Resonance in Medicine, 2018, 80, 802-813.	3.0	20
133	Automatic localization of EEG electrode markers within 3D MR data. Magnetic Resonance Imaging, 2000, 18, 485-488.	1.8	19
134	Altered diffusion tensor imaging measurements in aged transgenic Huntington disease rats. Brain Structure and Function, 2013, 218, 767-778.	2.3	19
135	Subchronic memantine induced concurrent functional disconnectivity and altered ultra-structural tissue integrity in the rodent brain: revealed by multimodal MRI. Psychopharmacology, 2013, 227, 479-491.	3.1	18
136	Intrinsic functional connectivity reduces after first-time exposure to short-term gravitational alterations induced by parabolic flight. Scientific Reports, 2017, 7, 3061.	3.3	18
137	Exploring sex differences in the adult zebra finch brain: In vivo diffusion tensor imaging and ex vivo super-resolution track density imaging. NeuroImage, 2017, 146, 789-803.	4.2	18
138	High quality statistical shape modelling of the human nasal cavity and applications. Royal Society Open Science, 2018, 5, 181558.	2.4	18
139	A Unified Maximum Likelihood Framework for Simultaneous Motion and \$T_{1}\$ Estimation in Quantitative MR \$T_{1}\$ Mapping. IEEE Transactions on Medical Imaging, 2017, 36, 433-446.	8.9	17
140	Brain Connectometry Changes in Space Travelers After Long-Duration Spaceflight. Frontiers in Neural Circuits, 2022, 16, 815838.	2.8	17
141	Automatic segmentation and modelling of two-dimensional electrophoresis gels. , 0, , .		16
142	A Multiresolution Approach to Discrete Tomography Using DART. PLoS ONE, 2014, 9, e106090.	2.5	16
143	Robust edge-directed interpolation of magnetic resonance images. Physics in Medicine and Biology, 2011, 56, 7287-7303.	3.0	15
144	Fast inline inspection by Neural Network Based Filtered Backprojection: Application to apple inspection. Case Studies in Nondestructive Testing and Evaluation, 2016, 6, 14-20.	1.7	15

#	Article	IF	CITATIONS
145	STAPP: Spatiotemporal analysis of plantar pressure measurements using statistical parametric mapping. Gait and Posture, 2018, 63, 268-275.	1.4	15
146	Implications of the Rician distribution for fMRI generalized likelihood ratio tests. Magnetic Resonance Imaging, 2005, 23, 953-959.	1.8	14
147	Likelihood-Based Hypothesis Tests for Brain Activation Detection From MRI Data Disturbed by Colored Noise: A Simulation Study. IEEE Transactions on Medical Imaging, 2009, 28, 287-296.	8.9	14
148	Dynamic angle selection in X-ray computed tomography. Nuclear Instruments & Methods in Physics Research B, 2014, 324, 17-24.	1.4	14
149	Region-Based Iterative Reconstruction of Structurally Changing Objects in CT. IEEE Transactions on Image Processing, 2014, 23, 909-919.	9.8	14
150	Neutron radiography and tomography applied to fuel degradation during ramp tests and loss of coolant accident tests in a research reactor. Progress in Nuclear Energy, 2014, 72, 55-62.	2.9	14
151	Chronic exposure to haloperidol and olanzapine leads to common and divergent shape changes in the rat hippocampus in the absence of grey-matter volume loss. Psychological Medicine, 2016, 46, 3081-3093.	4.5	14
152	Superâ€resolution <i>T</i> ₁ estimation: Quantitative high resolution <i>T</i> ₁ mapping from a set of low resolution <i>T</i> ₁ â€weighted images with different slice orientations. Magnetic Resonance in Medicine, 2017, 77, 1818-1830.	3.0	14
153	Posture normalisation of 3D body scans. Ergonomics, 2019, 62, 834-848.	2.1	14
154	Constrained spherical deconvolution of nonspherically sampled diffusion <scp>MRI</scp> data. Human Brain Mapping, 2021, 42, 521-538.	3.6	14
155	MoVIT: a tomographic reconstruction framework for 4D-CT. Optics Express, 2017, 25, 19236.	3.4	13
156	Super-Resolution Magnetic Resonance Imaging of the Knee Using 2-Dimensional Turbo Spin Echo Imaging. Investigative Radiology, 2020, 55, 481-493.	6.2	13
157	Feasibility and Advantages of Diffusion Weighted Imaging Atlas Construction in Q-Space. Lecture Notes in Computer Science, 2011, 14, 166-173.	1.3	13
158	Inline nondestructive internal disorder detection in pear fruit using explainable deep anomaly detection on X-ray images. Computers and Electronics in Agriculture, 2022, 197, 106962.	7.7	13
159	Imaging birds in a bird cage: in-vivo FSE 3D MRI of bird brain. Magnetic Resonance Materials in Physics, Biology, and Medicine, 1998, 6, 22-27.	2.0	12
160	Influence of User-Defined Parameters on Diffusion Tensor Tractography of the Corticospinal Tract. Neuroradiology Journal, 2007, 20, 139-147.	1.2	12
161	Glucocorticoid-Induced Osteoporosis in Growing Mice Is Not Prevented by Simultaneous Intermittent PTH Treatment. Calcified Tissue International, 2009, 85, 530-537.	3.1	12
162	Technical Note: A safe, cheap, and easyâ€ŧoâ€use isotropic diffusion <scp>MRI</scp> phantom for clinical and multicenter studies. Medical Physics, 2017, 44, 1063-1070.	3.0	12

#	Article	IF	CITATIONS
163	Generalized likelihood ratio tests for complex fMRI data: a Simulation study. IEEE Transactions on Medical Imaging, 2005, 24, 604-611.	8.9	11
164	Detecting and locating light atoms from high-resolution STEM images: The quest for a single optimal design. Ultramicroscopy, 2016, 170, 128-138.	1.9	11
165	Building 3D Statistical Shape Models of Horticultural Products. Food and Bioprocess Technology, 2017, 10, 2100-2112.	4.7	11
166	Methods for characterization and optimisation of measuring performance of stereoscopic x-ray systems with image intensifiers. Measurement Science and Technology, 2019, 30, 105701.	2.6	11
167	Joint Deblurring and Denoising of THz Time-Domain Images. IEEE Access, 2021, 9, 162-176.	4.2	11
168	D-BRAIN: Anatomically Accurate Simulated Diffusion MRI Brain Data. PLoS ONE, 2016, 11, e0149778.	2.5	11
169	CNN-based Deblurring of Terahertz Images. , 2020, , .		11
170	The effect of beam hardening on resolution in x-ray microtomography. , 2004, 5370, 2089.		10
171	Morphologic and functional changes in the unilateral 6-hydroxydopamine lesion rat model for Parkinson's disease discerned withÂμSPECT and quantitative MRI. Magnetic Resonance Materials in Physics, Biology, and Medicine, 2010, 23, 65-75.	2.0	10
172	An adaptive non local maximum likelihood estimation method for denoising magnetic resonance images. , 2012, , .		10
173	3D morphometric analysis of the human incudomallear complex using clinical cone-beam CT. Hearing Research, 2016, 340, 79-88.	2.0	10
174	Neural network Hilbert transform based filtered backprojection for fast inline x-ray inspection. Measurement Science and Technology, 2018, 29, 034012.	2.6	10
175	NOVIFAST: A Fast Algorithm for Accurate and Precise VFA MRI <inline-formula> <tex-math notation="LaTeX">\${T}_{1}\$ </tex-math </inline-formula> Mapping. IEEE Transactions on Medical Imaging, 2018, 37, 2414-2427.	8.9	10
176	Matlab® toolbox for semi-automatic segmentation of the human nasal cavity based on active shape modeling. Computers in Biology and Medicine, 2019, 105, 27-38.	7.0	10
177	Small medial femoral condyle morphotype is associated with medial compartment degeneration and distinct morphological characteristics: a comparative pilot study. Knee Surgery, Sports Traumatology, Arthroscopy, 2021, 29, 1777-1789.	4.2	10
178	On the generalizability of diffusion MRI signal representations across acquisition parameters, sequences and tissue types: Chronicles of the MEMENTO challenge. NeuroImage, 2021, 240, 118367.	4.2	10
179	Recurrent inference machines as inverse problem solvers for MR relaxometry. Medical Image Analysis, 2021, 74, 102220.	11.6	10
180	<title>Optimal estimation of T<formula><inf><roman>2</roman></inf></formula> maps from</td><td></td><td>9</td></tr></tbody></table></title>		

magnitude MR images</title>., 1998, 3338, 384.

#	Article	IF	CITATIONS
181	How to optimize the design of a quantitative HREM experiment so as to attain the highest precision. Journal of Microscopy, 1999, 194, 95-104.	1.8	9
182	A memory efficient method for fully three-dimensional object reconstruction with HAADF STEM. Ultramicroscopy, 2014, 141, 22-31.	1.9	9
183	Data-Driven Affine Deformation Estimation and Correction in Cone Beam Computed Tomography. IEEE Transactions on Image Processing, 2017, 26, 1441-1451.	9.8	9
184	White matter microstructural organisation of interhemispheric pathways predicts different stages of bimanual coordination learning in young and older adults. European Journal of Neuroscience, 2018, 47, 446-459.	2.6	9
185	Design smart clothing using digital human models. , 2019, , 683-698.		9
186	Supporting measurements or more averages? How to quantify cerebral blood flow most reliably in 5 minutes by arterial spin labeling. Magnetic Resonance in Medicine, 2020, 84, 2523-2536.	3.0	9
187	Subject-specific identification of three dimensional foot shape deviations using statistical shape analysis. Expert Systems With Applications, 2020, 151, 113372.	7.6	9
188	poly-DART: A discrete algebraic reconstruction technique for polychromatic X-ray CT. Optics Express, 2019, 27, 33670.	3.4	9
189	Evaluation of 3D Body Shape Predictions Based on Features. , 2015, , .		9
190	Deep learning-based 2D/3D registration of an atlas to biplanar X-ray images. International Journal of Computer Assisted Radiology and Surgery, 2022, 17, 1333-1342.	2.8	9
191	Automatic anomaly detection from X-ray images based on autoencoders. Nondestructive Testing and Evaluation, 2022, 37, 552-565.	2.1	9
192	Algorithm for the computation of 3D Fourier descriptors. , 0, , .		8
193	Multiscale watershed segmentation of multivalued images. , 0, , .		8
194	Combined Motion Estimation and Reconstruction in Tomography. Lecture Notes in Computer Science, 2012, , 12-21.	1.3	8
195	The reconstructed residual error: A novel segmentation evaluation measure for reconstructed images in tomography. Computer Vision and Image Understanding, 2014, 126, 28-37.	4.7	8
196	Modeling blurring effects due to continuous gantry rotation: Application to region of interest tomography. Medical Physics, 2015, 42, 2709-2717.	3.0	8
197	A three-dimensional digital neurological atlas of the mustached bat (Pteronotus parnellii). Neurolmage, 2018, 183, 300-313.	4.2	8
198	A low-cost geometry calibration procedure for a modular cone-beam X-ray CT system. Nondestructive Testing and Evaluation, 2020, 35, 252-265.	2.1	8

6

#	Article	IF	CITATIONS
199	The effect of nasal shape on the thermal conditioning of inhaled air: Using clinical tomographic data to build a large-scale statistical shape model. Computers in Biology and Medicine, 2020, 117, 103600.	7.0	8
200	Geometry Calibration of a Modular Stereo Cone-Beam X-ray CT System. Journal of Imaging, 2021, 7, 54.	3.0	8
201	Discrete tomography from micro-CT data: application to the mouse trabecular bone structure. , 2006, 6142, 1325.		7
202	Noise measurement from magnitude MRI using local estimates of variance and skewness. Physics in Medicine and Biology, 2010, 55, 6973-6973.	3.0	7
203	A discrete tomography approach for superresolution micro-CT images: application to bone. , 2010, , .		7
204	Discrete Tomography in MRI: a Simulation Study. Fundamenta Informaticae, 2013, 125, 223-237.	0.4	7
205	Pore REconstruction and Segmentation (PORES) method for improved porosity quantification of nanoporous materials. Ultramicroscopy, 2015, 148, 10-19.	1.9	7
206	Partial Discreteness: A Novel Prior for Magnetic Resonance Image Reconstruction. IEEE Transactions on Medical Imaging, 2017, 36, 1041-1053.	8.9	7
207	Atom-counting in High Resolution Electron Microscopy:TEM or STEM – That's the question. Ultramicroscopy, 2017, 174, 112-120.	1.9	7
208	Parametric Reconstruction of Glass Fiber-reinforced Polymer Composites from X-ray Projection Data—A Simulation Study. Journal of Nondestructive Evaluation, 2018, 37, 62.	2.4	7
209	PAPPI: Personalized analysis of plantar pressure images using statistical modelling and parametric mapping. PLoS ONE, 2020, 15, e0229685.	2.5	7
210	Diffusion tensor imaging of the anterior cruciate ligament following primary repair with internal bracing: A longitudinal study. Journal of Orthopaedic Research, 2021, 39, 1318-1330.	2.3	7
211	Monte-Carlo-Based Estimation of the X-ray Energy Spectrum for CT Artifact Reduction. Applied Sciences (Switzerland), 2021, 11, 3145.	2.5	7
212	Segmentation Based Noise Variance Estimation from Background MRI Data. Lecture Notes in Computer Science, 2010, , 62-70.	1.3	7
213	Model-based super-resolution reconstruction with joint motion estimation for improved quantitative MRI parameter mapping. Computerized Medical Imaging and Graphics, 2022, 100, 102071.	5.8	7
214	Diffusion tensor image up-sampling: a registration-based approach. Magnetic Resonance Imaging, 2010, 28, 1497-1506.	1.8	6
215	Assessment and stenting of tracheal stenosis using deformable shape models. Medical Image Analysis, 2011, 15, 250-266.	11.6	6

216 Fractional Eigenfaces. , 2014, , .

#	Article	IF	CITATIONS
217	Local attenuation curve optimization framework for high quality perfusion maps in lowâ€dose cerebral perfusion CT. Medical Physics, 2016, 43, 6429-6438.	3.0	6
218	An assessment of the information lost when applying data reduction techniques to dynamic plantar pressure measurements. Journal of Biomechanics, 2019, 87, 161-166.	2.1	6
219	Unveiling water dynamics in fuel cells from time-resolved tomographic microscopy data. Scientific Reports, 2020, 10, 16388.	3.3	6
220	Dynamic few-view X-ray imaging for inspection of CAD-based objects. Expert Systems With Applications, 2021, 180, 115012.	7.6	6
221	Estimation of Signal and Noise Parameters from MR Data. Signal Processing and Communications, 2005, , 85-143.	0.2	6
222	Multiscale anisotropic filtering of color images. , 0, , .		5
223	Estimation of uncertainty in constrained spherical deconvolution fiber orientations. , 2008, , .		5
224	Denoising Magnetic Resonance Images Using Fourth Order Complex Diffusion. , 2009, , .		5
225	Type-2 Fuzzy GMM-UBM for Text-Independent Speaker Verification. , 2013, , .		5
226	3D imaging of semiconductor components by discrete laminography. , 2014, , .		5
227	Discrete tomography in an in vivo small animal bone study. Journal of Bone and Mineral Metabolism, 2018, 36, 40-53.	2.7	5
228	Enhanced contrast in Xâ€ray microtomographic images of the membranous labyrinth using different Xâ€ray sources and scanning modes. Journal of Anatomy, 2018, 233, 770-782.	1.5	5
229	The costs and benefits of estimating T 1 of tissue alongside cerebral blood flow and arterial transit time in pseudoâ€continuous arterial spin labeling. NMR in Biomedicine, 2020, 33, e4182.	2.8	5
230	Quantification of cognitive impairment to characterize heterogeneity of patients at risk of developing Alzheimer's disease dementia. Alzheimer's and Dementia: Diagnosis, Assessment and Disease Monitoring, 2021, 13, e12237.	2.4	5
231	Extended imaging volume in cone-beam x-ray tomography using the weighted simultaneous iterative reconstruction technique. Physics in Medicine and Biology, 2021, 66, 165008.	3.0	5
232	Moving Statistical Body Shape Models Using Blender. Advances in Intelligent Systems and Computing, 2019, , 28-38.	0.6	5
233	Efficient algorithm fo the computation of 3D Fourier descriptors. , 0, , .		4

A new algorithm for 2D region of interest tomography. , 2004, , .

#	Article	IF	CITATIONS
235	Statistical Shape Modeling and Population Analysis of the Aortic Root of TAVI Patients. Journal of Medical Devices, Transactions of the ASME, 2013, 7, .	0.7	4
236	Adaptive zooming in X-ray computed tomography. Journal of X-Ray Science and Technology, 2014, 22, 77-89.	1.0	4
237	Can portable tomosynthesis improve the diagnostic value of bedside chest X-ray in the intensive care unit? A proof of concept study. European Radiology Experimental, 2017, 1, 20.	3.4	4
238	StatSTEM: An efficient program for accurate and precise model-based quantification of atomic resolution electron microscopy images. Journal of Physics: Conference Series, 2017, 902, 012013.	0.4	4
239	IntensityPatches and RegionPatches for image recognition. Applied Soft Computing Journal, 2018, 62, 176-186.	7.2	4
240	A Deep Learning Approach to Horse Bone Segmentation from Digitally Reconstructed Radiographs. , 2019, , .		4
241	Diffusion tensor imaging of the anterior cruciate ligament graft following reconstruction: a longitudinal study. European Radiology, 2020, 30, 6673-6684.	4.5	4
242	Joint Maximum Likelihood Estimation of Motion and T1 Parameters from Magnetic Resonance Images in a Super-resolution Framework: a Simulation Study. Fundamenta Informaticae, 2020, 172, 105-128.	0.4	4
243	Analysis and comparison of algorithms for the tomographic reconstruction of curved fibres. Nondestructive Testing and Evaluation, 2020, 35, 328-341.	2.1	4
244	The Gated Recurrent Conditional Generative Adversarial Network (GRC-GAN): application to denoising of low-dose CT images. , 2021, , .		4
245	3D total variation denoising in X-CT imaging applied to pore extraction in additively manufactured parts. Measurement Science and Technology, 2022, 33, 045602.	2.6	4
246	Improved diffusion parameter estimation by incorporating T2 relaxation properties into the DKI-FWE model. NeuroImage, 2022, 256, 119219.	4.2	4
247	Robust edge-directed interpolation of magnetic resonance images. , 2011, , .		3
248	Neural netwok based X-ray tomography for fast inspection of apples on a conveyor belt system. , 2015, ,		3
249	Pixel Clustering for Face Recognition. , 2016, , .		3
250	Diffusion Kurtosis Imaging. , 2016, , 407-418.		3
251	A nonlocal maximum likelihood estimation method for enhancing magnetic resonance phase maps. Signal, Image and Video Processing, 2017, 11, 913-920.	2.7	3
252	A Visual Tool for the Analysis of Algorithms for Tomographic Fiber Reconstruction in Materials Science. Computer Graphics Forum, 2019, 38, 273-283.	3.0	3

JAN SIJBERS

#	Article	IF	CITATIONS
253	Adaptable digital human models from 3D body scans. , 2019, , 459-470.		3
254	The Radon Transform For Terahertz Computed Tomography Incorporating The Beam Shape. , 2020, , .		3
255	A Machine Learning Approach to Growth Direction Finding for Automated Planting of Bulbous Plants. Scientific Reports, 2020, 10, 661.	3.3	3
256	Accelerating in vivo fast spin echo high angular resolution diffusion imaging with an isotropic resolution in mice through compressed sensing. Magnetic Resonance in Medicine, 2021, 85, 1397-1413.	3.0	3
257	To recurse or not to recurse: a low-dose CT study. Progress in Artificial Intelligence, 2021, 10, 65-81.	2.4	3
258	Analysis Of Flat Fields In Edge Illumination Phase Contrast Imaging. , 2021, , .		3
259	Adjoint image warping using multivariate splines with application to fourâ€dimensional computed tomography. Medical Physics, 2021, 48, 6362-6374.	3.0	3
260	A New Nonlocal Maximum Likelihood Estimation Method for Denoising Magnetic Resonance Images. Lecture Notes in Computer Science, 2013, , 451-458.	1.3	3
261	Imaging birds in a bird cage: in-vivo FSE 3D MRI of bird brain. Magnetic Resonance Materials in Physics, Biology, and Medicine, 1998, 6, 22-27.	2.0	2
262	Robust estimation of the noise variance from background MR data. , 2006, , .		2
263	Automatic local thresholding of tomographic reconstructions based on the projection data. , 2008, , .		2
264	Susceptibility correction for improved tractography using high field DT-EPI. Proceedings of SPIE, 2008,	0.8	2
265	Bias field reduction by localized Lloyd–Max quantization. Magnetic Resonance Imaging, 2011, 29, 536-545.	1.8	2
266	Optimized workflow for diffusion kurtosis imaging of newborns. , 2011, , .		2
267	Quantitative evaluation of ASiR image quality: an adaptive statistical iterative reconstruction technique. , 2012, , .		2
268	Discrete algebraic reconstruction technique: a new approach for superresolution reconstruction of license plates. Journal of Electronic Imaging, 2013, 22, 041111.	0.9	2
269	Type-2 Fuzzy GMMs for Robust Text-Independent Speaker Verification in Noisy Environments. , 2014, , .		2
270	Filtered backprojection using algebraic filters; application to biomedical micro-CT data. , 2015, , .		2

#	Article	IF	CITATIONS
271	Simultaneous motion correction and T <inf>1</inf> estimation in quantitative T <inf>1</inf> mapping: An ML restoration approach. , 2015, , .		2
272	A multi-level preconditioned Krylov method for the efficient solution of algebraic tomographic reconstruction problems. Journal of Computational and Applied Mathematics, 2015, 283, 1-16.	2.0	2
273	Investigation on the effect of exposure time on scintillator afterglow for ultra-fast tomography acquisition. Journal of Instrumentation, 2016, 11, C12014-C12014.	1.2	2
274	X-ray Phase-contrast Simulations of Fibrous Phantoms using GATE. , 2018, , .		2
275	Advanced x-ray tomography: experiment, modeling, and algorithms. Measurement Science and Technology, 2018, 29, 080101.	2.6	2
276	A Comparative Study Between Three Measurement Methods to Predict 3D Body Dimensions Using Shape Modelling. Advances in Intelligent Systems and Computing, 2020, , 464-470.	0.6	2
277	Accurate Terahertz Imaging Simulation With Ray Tracing Incorporating Beam Shape and Refraction. , 2020, , .		2
278	EquiSim: An Open-Source Articulatable Statistical Model of the Equine Distal Limb. Frontiers in Veterinary Science, 2021, 8, 623318.	2.2	2
279	CAD-Based Scatter Compensation For Polychromatic Reconstruction Of Additive Manufactured Parts. , 2021, , .		2
280	A Combined Statistical Shape Model of the Scalp and Skull of the Human Head. Advances in Intelligent Systems and Computing, 2018, , 538-548.	0.6	2
281	Segmentation of the Human Trachea Using Deformable Statistical Models of Tubular Shapes. , 2007, , 531-542.		2
282	Projection-angle-dependent distortion correction in high-speed image-intensifier-based x-ray computed tomography. Measurement Science and Technology, 2021, 32, 035404.	2.6	2
283	Fiber assignment by continuous tracking for parametric fiber reinforced polymer reconstruction. , 2019, , .		2
284	Foot Abnormality Mapping using Statistical Shape Modelling. , 0, , .		2
285	A Likelihood Ratio Test for Functional MRI Data Analysis to Account for Colored Noise. Lecture Notes in Computer Science, 2005, , 538-546.	1.3	2
286	Improved Shape Modeling of Tubular Objects Using Cylindrical Parameterization. Lecture Notes in Computer Science, 2006, , 84-91.	1.3	2
287	Automatic multiple threshold scheme for segmentation of tomograms. , 2007, , .		2
288	A Bottom-Up Volume Reconstruction Method for Atom Probe Tomography. Microscopy and Microanalysis, 2022, 28, 1102-1115.	0.4	2

#	Article	IF	CITATIONS
289	Multi-contrast multi-shot EPI for accelerated diffusion MRI. , 2021, 2021, 3869-3872.		2
290	Probability of detection applied to X-ray inspection using numerical simulations. Nondestructive Testing and Evaluation, 2022, 37, 536-551.	2.1	2
291	<title>Volume quantization of the mouse cerebellum by semiautomatic 3D segmentation of magnetic resonance images</title> . , 1996, , .		1
292	<title>MRI as a tool to study brain structure from mouse models for mental retardation</title> . , 1998, , .		1
293	<title>Adaptive anisotropic noise filtering for magnitude MR data</title> . , 1999, 3661, 1418.		1
294	Maximum likelihood estimation of signal amplitude and noise variance from complex valued data. IFAC Postprint Volumes IPPV / International Federation of Automatic Control, 2003, 36, 127-132.	0.4	1
295	Diffusion Tensor Images Upsampling: A Registration-Based Approach. , 2009, , .		1
296	Improved B0 field map estimation for high field EPI. Magnetic Resonance Imaging, 2010, 28, 441-450.	1.8	1
297	Diffusion tensor images edge-directed interpolation. , 2010, , .		1
298	Benefits and shortcomings of partial volume interpolation for MI based image registration. , 2010, , .		1
299	A maximum likelihood estimation method for denoising magnitude MRI using restricted local neighborhood. Proceedings of SPIE, 2011, , .	0.8	1
300	Force Feedback to Assist Active Contour Modelling for Tracheal Stenosis Segmentation. Advances in Human-Computer Interaction, 2012, 2012, 1-9.	2.8	1
301	Motion Compensation Techniques in Permutation-Based Video Encryption. , 2013, , .		1
302	Aligning Projection Images from Binary Volumes. Fundamenta Informaticae, 2014, 135, 21-42.	0.4	1
303	Region based 4D tomographic image reconstruction: Application to cardiac x-ray CT. , 2015, , .		1
304	Understanding microstructural deformation of apple tissue from 4D micro-CT imaging. Acta Horticulturae, 2018, , 7-14.	0.2	1
305	Joint Reconstruction and Flat-Field Estimation using Support Estimation. , 2018, , .		1
306	Multi-patch B-Spline Statistical Shape Models for CAD-Compatible Digital Human Modeling. Advances in Intelligent Systems and Computing, 2019, , 179-189.	0.6	1

JAN SIJBERS

#	Article	IF	CITATIONS
307	Aortic root sizing for transcatheter aortic valve implantation using a shape model parameterisation. Medical and Biological Engineering and Computing, 2019, 57, 2081-2092.	2.8	1
308	Newton-Krylov Methods For Polychromatic X-Ray CT. , 2020, , .		1
309	Outlier Detection for Foot Complaint Diagnosis: Modeling Confounding Factors Using Metric Learning. IEEE Intelligent Systems, 2021, 36, 41-49.	4.0	1
310	Parameter estimation from magnitude MR images. , 1999, 10, 109.		1
311	Quantifying cognition and behavior in normal aging, mild cognitive impairment, and Alzheimer's disease. , 2017, , .		1
312	Threshold Selection for Segmentation of Dense Objects in Tomograms. Lecture Notes in Computer Science, 2008, , 700-709.	1.3	1
313	An Articulating Statistical Shape Model of the Human Hand. Advances in Intelligent Systems and Computing, 2019, , 433-445.	0.6	1
314	Automatic Generation of Statistical Shape Models in Motion. Advances in Intelligent Systems and Computing, 2019, , 170-178.	0.6	1
315	Dynamic angle selection for few-view X-ray inspection of CAD based objects. , 2019, , .		1
316	Colon Visualization Using Cylindrical Parameterization. , 2007, , 607-615.		1
317	Selection of Local Thresholds for Tomogram Segmentation by Projection Distance Minimization. , 2008, , 380-391.		1
318	Fracture patterns in midshaft clavicle fractures. Acta Orthopaedica Belgica, 2021, 87, 501-507.	0.4	1
319	Gauss-Newton-Krylov for Reconstruction of Polychromatic X-Ray CT Images. IEEE Transactions on Computational Imaging, 2021, 7, 1304-1313.	4.4	1
320	<title>Maximum-likelihood signal estimation in phase contrast magnitude MR images</title> . , 1998, , .		0
321	Dose Limited Resolution. Microscopy and Microanalysis, 1998, 4, 802-803.	0.4	Ο
322	Towards Quantitative Structure Determination Through Electron Holographic Methods. Materials Characterization, 1999, 42, 265-281.	4.4	0
323	<title>Automatic detection of EEG electrode markers on 3D MR data</title> . , 2000, , .		0
324	<title>Automatic EEG signal restoration during simultaneous EEG/MR acquisitions</title> ., 2000, , .		0

#	Article	IF	CITATIONS
325	<title>Changes during pentetrazol-induced epilepsy in rat recorded by simultaneous EEG/MRI at
7T</title> . , 2000, 3978, 485.		0
326	A bimodal energy model for correcting beam hardening artefacts in X-ray tomography. , 0, , .		0
327	Generalized likelihood ratio tests for complex fMRI data. , 2004, , .		Ο
328	Discrete tomography: exploiting various forms of discreteness in electron tomography. Microscopy and Microanalysis, 2008, 14, 1050-1051.	0.4	0
329	Tracheal stent prediction using statistical deformable models of tubular shapes. Proceedings of SPIE, 2008, , .	0.8	0
330	Seeing through the window: pre-fetching strategies for out-of-core image processing algorithms. , 2008, , .		0
331	The evaluation of a population based diffusion tensor image atlas using a ground truth method. Proceedings of SPIE, 2008, , .	0.8	0
332	Fast bias field reduction by localized Lloyd-Max quantization. , 2008, , .		0
333	An exploration of spatial similarities in temporal noise spectra in fMRI measurements. , 2008, , .		0
334	Non-rigid coregistration of diffusion kurtosis data. , 2010, , .		0
335	Pedestrian Detection under Progressive Occlusion. , 2013, , .		0
336	A Combined Features Approach for Speaker Segmentation Using BIC and Artificial Neural Networks. , 2013, , .		0
337	Alveolar Nerve Unfolding Technique for Synoptic Analysis. Journal of Craniofacial Surgery, 2013, 24, e374-e377.	0.7	0
338	Statistical Shape Modeling and Population Analysis of the Aortic Root of TAVI Patients. , 2013, , .		0
339	Conveyor Belt X-ray CT Using Domain Constrained Discrete Tomography. , 2014, , .		0
340	Partially discrete magnetic resonance tomography. , 2015, , .		0
341	High resolution T1 estimation from multiple low resolution magnetic resonance images. , 2015, , .		0
342	Multi-voxel algorithm for quantitative bi-exponential MRI T ₁ estimation. Proceedings of SPIE, 2016, , .	0.8	0

1.00	~		
ΛN	SIJ	RF	DC
	JU		r S

#	Article	IF	CITATIONS
343	TCT-465 Automatic Identification and Quantification of the Mitral Annulus for Consistent TMVR Planning: A Preliminary Study. Journal of the American College of Cardiology, 2019, 74, B460.	2.8	0
344	Normalized averaged range (nAR), a robust quantification method for MPIO-content. Journal of Magnetic Resonance, 2019, 300, 18-27.	2.1	0
345	Statistical Shape and Pose Model of the Forearm for Custom Splint Design. , 2021, , .		0
346	DART explained: how to carry out a discrete tomography reconstruction. , 2008, , 295-296.		0
347	Experiences with Cell-BE and GPU for Tomography. Lecture Notes in Computer Science, 2009, , 298-307.	1.3	0
348	Changes in intrinsic functional brain connectivity after first-time exposure to parabolic flight Frontiers in Physiology, 0, 9, .	2.8	0
349	CNN-based Pose Estimation of Manufactured Objects During Inline X-ray Inspection. , 2021, , .		0
350	Extreme Sparse X-ray Computed Laminography Via Convolutional Neural Networks. , 2020, , .		0
351	Using particle systems for mitral valve segmentation from 3D transoesophageal echocardiography (3D) Tj ETQq1 Visualization, 0, , 1-9.	1 0.78431 1.9	l4 rgBT /O 0
352	Title is missing!. , 2020, 15, e0229685.		0
353	Title is missing!. , 2020, 15, e0229685.		0
354	Title is missing!. , 2020, 15, e0229685.		0
355	Title is missing!. , 2020, 15, e0229685.		0